Real-time change detection of steady-state evoked potentials

Gideon Nave, Yonina C. Eldar, Gideon Inbar, Alon Sinai, Hillel Pratt & Menashe Zaaroor

Biological Cybernetics
Advances in Computational Neuroscience

ISSN 0340-1200
Volume 107
Number 1

Biol Cybern (2013) 107:49-59
DOI 10.1007/s00422-012-0523-5

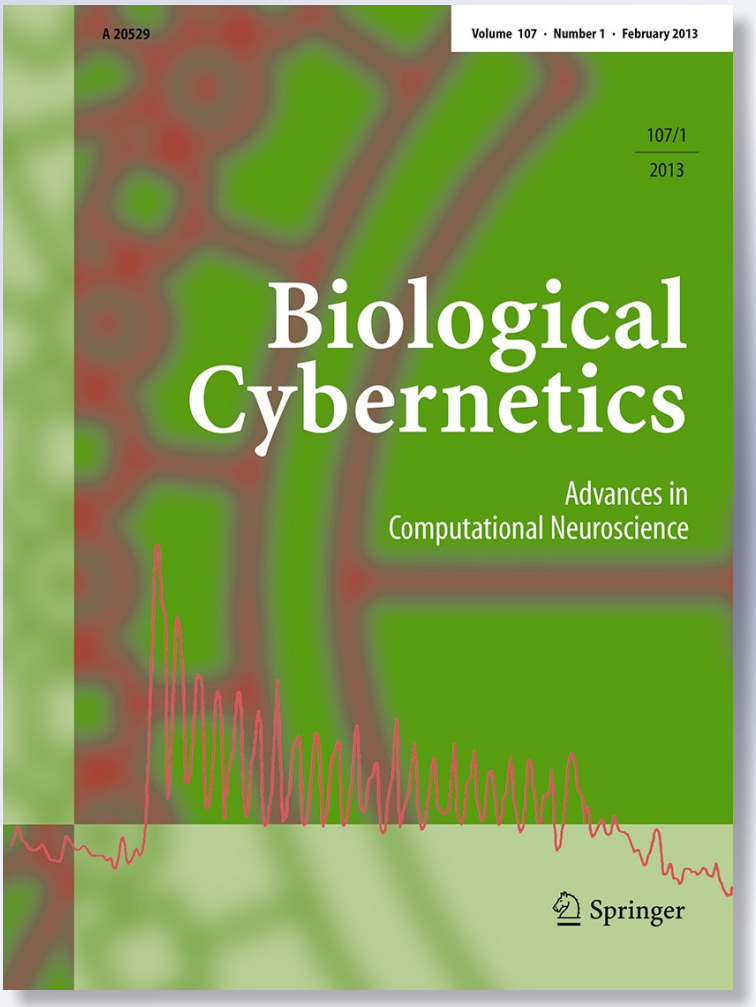

Springer

Biol Cybern (2013) 107:49–59
DOI 10.1007/s00422-012-0523-5

ORIGINAL PAPER

Biological Cybernetics

Real-time change detection of steady-state evoked potentials

Gideon Nave · Yonina C. Eldar · Gideon Inbar · Alon Sinai · Hillel Pratt · Menashe Zaaroor

Received: 1 November 2011 / Accepted: 18 September 2012 / Published online: 5 October 2012

Abstract Steady-state evoked potentials (SSEP) are the electrical activity recorded from the scalp in response to high-rate sensory stimulation. SSEP consist of a constituent frequency component matching the stimulation rate, whose amplitude and phase remain constant with time and are sensitive to functional changes in the stimulated sensory system. Monitoring SSEP during neurosurgical procedures allows identification of an emerging impairment early enough before the damage becomes permanent. In routine practice, SSEP are extracted by averaging of the EEG recordings, allowing detection of neurological changes within approximately a minute. As an alternative to the relatively slow-responding empirical averaging, we present an algorithm that detects changes in the SSEP within seconds. Our system alerts when changes in the SSEP are detected by applying a two-step Generalized Likelihood Ratio Test (GLRT) on the unaveraged EEG recordings. This approach outperforms conventional detection and provides the monitor with a statistical measure of the likelihood that a change occurred, thus enhancing its sensitivity and reliability. The system's performance is analyzed using Monte Carlo simulations and tested on real EEG data recorded under coma.

Keywords Evoked potentials · Neuro-monitoring · Change detection · GLRT

Hillel Pratt and Menashe Zaaroor contributed equally to this study.

G. Nave (✉) · Y. C. Eldar · G. Inbar
Faculty of Electrical Engineering, Technion-IIT,
32000 Haifa, Israel
e-mail: gnave@caltech.edu

Y. C. Eldar
e-mail: yonina@ee.technion.ac.il

G. Inbar
e-mail: inbar@ee.technion.ac.il

G. Nave
Department of Computation and Neural Systems,
California Institute of Technology, Mail stop 228-77,
Pasadena, CA 91125, USA

A. Sinai · M. Zaaroor
Department of Neurosurgery, Rambam Health Care Campus
and Faculty of Medicine, Technion-IIT, Haifa, Israel
e-mail: a_sinai@rambam.health.gov.il

M. Zaaroor
e-mail: m_zaaroor@rambam.health.gov.il

H. Pratt
Evoked Potentials Laboratory, Faculties of Medicine,
and Biomedical Engineering, Technion-IIT, Haifa, Israel
e-mail: hillel@techunix.technion.ac.il

1 Introduction

Evoked potentials (EP) are the electrical potential generated by the activity of neurons in the brain, and recorded from a human or animal following presentation of a stimulus. EP amplitudes are typically in the order of a microvolt, compared to tens or hundreds of microvolts for spontaneous EEG. EP consist of three major types according to the sensory system activated: auditory, visual and somatosensory EP. Steady-state evoked potential (SSEP) are recorded in response to a stimulus repetition rate that is sufficiently high and the response is recorded with a sweep duration of several times the inter-stimulus interval. The amplitude and phase of constituent frequency components matching the rate of stimulation in the response, remain constant with time, and a train of repetitive sinusoidal waves is seen in the EP recordings as shown in Fig. 1 (Chiappa 1997). Each peak of the SSEP appears at some latency from the stimulus that evoked it. The latency difference is expressed as a phase lag between the stimulus and the peaks in the SSEP. SSEP are used in a

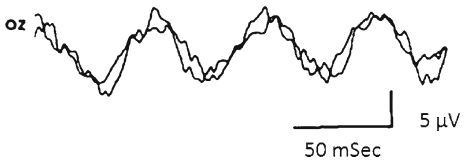

Fig. 1 Steady-state visual evoked potential waveforms recorded from electrodes Oz-A1 in response to a 20-Hz stimulus (Chiappa 1997). The waveform was obtained by averaging potentials in response to 512 stimuli.

variety of clinical applications, including assessing auditory and visual acuity in infants and adults unable to provide reliable verbal responses, detection of cortical blindness, and Brain–Computer Interface (see Heckenlively and Arden 1991; Middendorf et al. 2000; Friman et al. 2007).

Nowadays, EP monitoring is routine in surgical procedures placing sensory pathways at risk (Nuwer et al. 1995; Burke et al. 1999). Monitoring is typically performed by a neurophysiologist attending the surgery and provides means of identification of emerging neurologic impairment early enough before the damage becomes permanent, allowing corrective measures during the limited time window during which damage is reversible. Intra-operative monitoring aids the surgeon in identifying neural tissue around and in a tumor, by manipulating it and observing whether the EP is altered. Such monitoring provides reassurance to the surgeon when indicating that complications are unlikely to have occurred. As during most neurosurgical procedures the patient is anesthetized, EP provides the surgeon with relevant real-time information about the patients' sensory functions (Nuwer et al. 1993).

It has been shown that the amplitude and phase of the SSEP can monitor the patient's functional state during a surgical brain procedure (see Zaaroor et al. 1993; Wiedemayer et al. 2004; Bergholz et al. 2008). The measurements are sensitive to changes in the relevant sensory system, respond to such changes within seconds, and do not produce false alarms in surgical procedures that do not affect the sensory pathway or the brain in general. As an alternative to the widely used and relatively slow-responding (in the order of a minute, at best) averaging in the acquisition of SSEP, we present a system for real-time monitoring of SSEP, whose high-level structure is described in Fig. 2. During surgery, the patient's sensory system is stimulated using light flashes from goggle-mounted LEDs (Pratt et al. 1994) or auditory clicks from earphones, and the raw EEG data are recorded using scalp electrodes. The core of the system is an algorithm that detects real-time changes in the amplitude and phase of the SSEP, and alarms the surgeon when a change has likely occurred.

The rest of this article is organized as follows. We formulate the problem and review previous monitoring approaches in Sect. 2. We present our algorithm in Sect. 3 and demonstrate its performance in comparison to other methods using

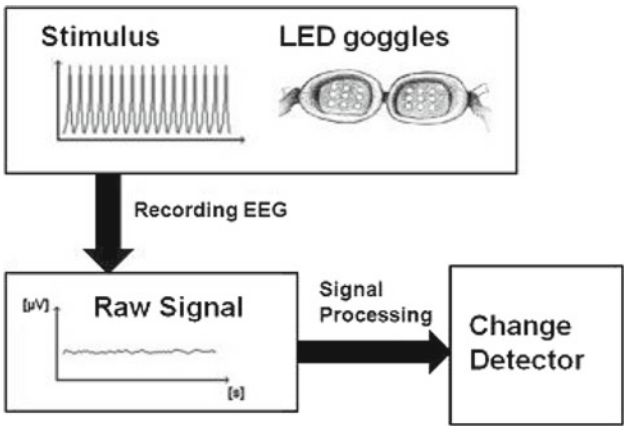

Fig. 2 SSEP monitoring system. During stimulation with the LED-goggles the raw EEG response is recorded. The recorded data serves as the input of the change detector that detects changes of the SSEP in real time

Monte Carlo simulations in Sect. 4. Experimental results of real human EEG data are presented in Sect. 5, followed by computational complexity analysis in Sect. 6. The study is concluded in Sect. 7, which includes a discussion and future research directions.

2 Problem definition and related work

Our signal model is based on a single EEG channel, as placing more electrodes on the skull may be inconvenient during brain-surgery.

SSEP is a digital signal of the form

$$s[n] = A[n]\cos\left(\omega_s n + \varphi[n]\right), \tag{1}$$

where $n = 1, 2, \ldots, M$ is the sample index and M denotes the number of data samples. $A[n]$ and $\varphi[n]$ are the SSEP amplitude and phase, respectively, and ω_s is the known stimulus frequency. Using complex exponents, the SSEP can be written as

$$s[n] = C[n]e^{j\omega_s n} + \bar{C}[n]e^{-j\omega_s n}, \tag{2}$$

where $|C[n]| = \frac{1}{2}A[n]$ and $\angle C[n] = \varphi[n]$. In order to keep track of changes in the amplitude and phase of the SSEP, we are interested in monitoring the variations of $C[n]$ over time.

The recorded EEG raw data are a digital signal, sampled at a frequency f, and modeled as

$$y[n] = s[n] + w[n], \tag{3}$$

where $y[n]$ is the EEG raw data, $s[n]$ is the SSEP and $w[n]$ is spontaneous EEG background. We assume that $y[n]$ was sampled from a band-limited analog EEG signal, such that the sampling rate f is sufficiently high for perfect reconstruction according to Nyquist–Shannon sampling theorem. In order

to allow real-time processing, we require that $f \leq f_{\text{proc}}$, where f_{proc} is the real-time processing rate, constrained by hardware limitations.

The first stimulus occurs at $n = 1$ and the sampling rate f is chosen to allow an integer number of samples per intra-stimulus period, given by N_T

$$N_T = \frac{2\pi f}{\omega_s}. \tag{4}$$

An SSEP change in sample N is defined as

$$\begin{cases} C[n] = C_0 \ \forall n \leq N \\ C[n] = C_1 \ \forall n > N, \end{cases} \tag{5}$$

where C_0 is a known complex scalar, $C_1 \neq C_0$ is an unknown complex scalar, and each time instant only one change has to be considered.

For convenience in the sequel, we define k as an integer constant, and the vector $\mathbf{v}$ as the kN_T-length vector of a harmonic signal at the stimulus frequency, whose lth element is given by

$$v[l] = e^{j\omega_s l}, \quad 1 \leq l < kN_T. \tag{6}$$

As we discuss SSEP monitoring methods, we note that all previous approaches base detection of changes on subjective manual interpretation of an estimated signal, regardless of statistical test of the probability that a change has occurred. Furthermore, all methods presume that the SSEP is constant over a time window which is sufficient for reliable estimation; in practice, however, the signal may change during this time window. Thus, monitoring suffers from unnecessary delays in high SNR conditions (when the estimation time window is set to be longer than needed), and on the other hand, estimation's accuracy may be insufficient for manual interpretation in low SNR scenarios. In order to allow reliable comparison between the different monitoring methods, we denote the duration of the above mentioned time window as T seconds. T is fully determined before the surgical procedure, according to the values of each method's parameters. Finally, none of the methods utilizes prior statistical knowledge that can be assumed about human EEG data recorded during anesthesia. The performance of all methods in comparison to our algorithm is discussed in Sect. 4.3.

2.1 Moving Empirical Average

Let $\mathbf{y}_p$ be the kN_T-length vector representing the recorded EEG following the pth stimulus

$$\mathbf{y}_p[l] = y[pN_T + l], \quad 1 \leq l < kN_T. \tag{7}$$

Based on (3), $\mathbf{y}_p$ is modeled as

$$\mathbf{y}_p[l] = \mathbf{s}_p[l] + \mathbf{w}_p[l], \tag{8}$$

where $\mathbf{s}_p$ is the SSEP and $\mathbf{w}_p$ is additive noise due to spontaneous EEG. The method assumes that the noise component is uncorrelated, zero-mean and uncorrelated with the signal (assumptions which are not entirely valid at all times, see McGillem et al. 1985). Based on an additional permise, that the SSEP has remained constant in the past N_A trials (which correspond to a time window of $T = \frac{kN_T}{f} N_A$ seconds), $\mathbf{s}_p$ is estimated by the empirical average $\bar{\mathbf{s}}_p$ (Gevins 1984)

$$\bar{\mathbf{s}}_p = \frac{1}{N_A} \sum_{q=0}^{N_A-1} \mathbf{y}_{p-qkN_T}. \tag{9}$$

During surgical procedures, $\bar{\mathbf{s}}_p$ waveform is updated after each stimulus, and the SSEP amplitude and phase are estimated by

$$|\hat{C}[p]| = \frac{1}{2} \max \bar{\mathbf{s}}_p \tag{10}$$

$$\angle \hat{C}[p] = \frac{2\pi}{N_T} \arg\max_l \bar{\mathbf{s}}_p[l] \mod N_T. \tag{11}$$

The variations of $C[p]$ are then interpreted by a neurophysiologist, manually detecting changes of the SSEP from its baseline before surgery (Wiedemayer et al. 2004).

2.2 Moving Subspace Average

Increasing the SNR obtained by empirical average can be achieved by computing its orthogonal projection onto the signal subspace.

$$\hat{\mathbf{s}}_p = [\mathbf{v}(\mathbf{v}^T\mathbf{v})^{-1}\mathbf{v}^T + \bar{\mathbf{v}}(\bar{\mathbf{v}}^T\bar{\mathbf{v}})^{-1}\bar{\mathbf{v}}^T]\bar{\mathbf{s}}_p, \tag{12}$$

where $\mathbf{v}$ is the vector defined by (6). Davila and Srebro (2000) used subspace averaging for estimating visual SSEP derived via counter-phase modulated contrast gratings. The method has never been used for intra-operative monitoring of SSEP; if it were used, the procedure would require manual interpretation of $C[p]$ measurements, that can be calculated using (10) and (11). Subspace averaging is expected to reduce the estimation period, and thus the system's delay of the empirical average, due to its improved SNR.

2.3 Real-Time Fourier Analysis

The mth frequency coefficient of the Discrete Fourier Transform (DFT) is defined as

$$Y_m = \frac{1}{N_W} \sum_{l=n-N_W+1}^{n} y[l] e^{-\frac{2\pi j}{N_W} ml}, \tag{13}$$

where both n and the transform window size, N_W, must be integer multiples of N_T. The SSEP is monitored using the

coefficient $m_s = \frac{N_W \omega_s}{2\pi f}$, which corresponds to the stimulus frequency, by

$$\hat{C}[n] = Y_{m_s}[n] \tag{14}$$

$C[n]$ variations are interpreted manually for detecting changes (see Bach 1999; Bergholz et al. 2008). DFT monitoring requires the assumption that the SSEP has remained constant over the last $T = \frac{N_W}{f}$ seconds.

2.4 Lock-in amplifier

When a sinusoidal function of frequency ω_1 is multiplied by another sinusoidal function of frequency ω_2 and integrated over a time much longer than the period of the two functions, the result is zero. In the case where $\omega_1 = \omega_2$ and the two functions are in phase, the average value equals half the product of the amplitudes (Scofield 1994). The lock-in operation is (Schacham and Pratt 1995)

$$X[n] = \frac{2}{N_L} \sum_{l=n-N_L+1}^{n} y[l] \cdot \cos(\omega_s l), \tag{15}$$

$$Y[n] = \frac{2}{N_L} \sum_{l=n-N_L+1}^{n} y[l] \cdot \sin(\omega_s l), \tag{16}$$

where $X[n]$ is the in-phase and $Y[n]$ is the out-of-phase SSEP components, and N_L is the averaging window. The method assumes that the SSEP has remained constant during the past $T = \frac{N_L}{f}$ seconds; its amplitude and phase are estimated by

$$|\hat{C}[n]| = \frac{1}{2}\sqrt{X[n]^2 + Y[n]^2}, \tag{17}$$

$$\angle \hat{C}[n] = \arctan \frac{Y[n]}{X[n]}. \tag{18}$$

Zaaroor et al. (1993) used analog lock-in amplifiers during neuro-surgical operations by manually interpreting the constantly updated SSEP amplitude and phase estimates.

In the following section, we present a method for detecting changes in the SSEP during surgery, based on the GLRT. Our approach overcomes the disadvantages of estimation methods, by utilizing statistical knowledge about human EEG during anesthesia for a post-processing change detection step, which is based on a flexible time window of measurements.

3 Change detection algorithm

Our approach addresses the problem definition in Sect. 2 and consists of four main stages, as described in Fig. 3. Before surgery, we estimate the SSEP baseline C_0. In order to follow the time variation of the signal during surgery, we split the recorded EEG raw data into short duration segments, in each of which we assume that the signal remained constant. Then, we calculate the Maximum Likelihood (ML) estimator of the SSEP in each segment, exploiting prior statistical knowledge on human EEG during anesthesia. Finally, we base change detection on a two-step GLRT applied on a flexible number of ML estimators, reducing delays in high SNR conditions and allowing to base detection on sufficient number of segments in low SNR conditions.

We assume that the parameter C is known and constant before surgery, as evident in clinical literature (Zaaroor et al. 1993). Its initial value, C_0, is estimated using the Subspace Averaging Method (see Sect. 2.2).

We split the raw EEG data into segments in which the parameter C is assumed to remain constant; the ith segment, $\mathbf{y}_i$, is a kN_T-length vector whose lth element is given by

$$\mathbf{y}_i[l] = y[ikN_T + l], \quad 1 \le l < kN_T. \tag{19}$$

Based on (3), $\mathbf{y}_i$ can be modeled as

$$\mathbf{y}_i[l] = \mathbf{s}_i[l] + \mathbf{w}_i[l], \tag{20}$$

such that $\mathbf{w}_i$ is the background EEG, and the SSEP equals to

$$\mathbf{s}_i = c_i \mathbf{v} + \bar{c}_i \bar{\mathbf{v}}, \tag{21}$$

where c_i is constant for each value of i.

Human EEG segments during anesthesia as short as 10 s can be modeled as zero mean stationary Gaussian random process (Bender et al. 1992). Furthermore, this model is not affected by adding a low level harmonic signal (Davilla et al. 1997). Hence, $\mathbf{w}_i$ can be modeled as

$$\mathbf{w}_i \sim \mathcal{N}(0, \mathbf{\Sigma}_i). \tag{22}$$

The covariance matrix $\mathbf{\Sigma}_i$ is unknown. Yet, it can be estimated by $\hat{\mathbf{\Sigma}}_i$, based on the raw data of the last 10 s of EEG recordings, using the auto-correlation estimation method (Orfanidis 1996). We use the stationarity of the EEG to estimate the covariance matrix as a Toepliz matrix, whose $[q, t]$ element equals to

$$\hat{\Sigma}_i[q,t] = \frac{1}{N_\Sigma - |q-t|} \sum_{n=0}^{N_\Sigma - |q-t| - 1} y_n \overline{y_{n+|q-t|}}, \tag{23}$$

where $N_\Sigma = 10f$ is the number of EEG samples in 10 s. As short EEG segments can be approximated by an auto-regressive (AR) processes (Bender et al. 1992), these values are decaying exponentially and can be set to zero for large values of $|q - t|$, that are greater than twice the AR model order, denoted by p.

The ML estimator of c_i in each segment, $\hat{c}_i$, is

$$\hat{c}_i = (\mathbf{v}^T {\mathbf{\Sigma}_i}^{-1} \mathbf{v})^{-1} \mathbf{v}^T {\mathbf{\Sigma}_i}^{-1} \mathbf{y}_i \tag{24}$$

$\hat{c}_i$ are random Gaussian variables, with

$$E(\hat{c}_i) = c_i \tag{25}$$

$$\mathrm{Var}(\hat{c}_i) = \frac{1}{\mathbf{v}^T {\Sigma_i}^{-1} \mathbf{v}} = \sigma_i^2. \tag{26}$$

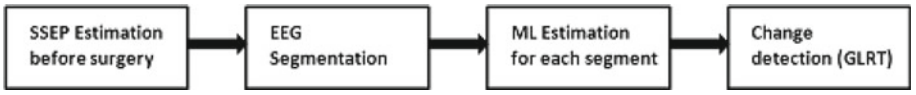

Fig. 3 A high-level block diagram of the SSEP real-time change detection algorithm

We use prior knowledge about the SSEP amplitude and regard ML estimators whose amplitudes are greater than the variance of the EEG signal before surgery as unreliable, by setting their variance, σ_i^2 to infinity.

Considering l as the index of the current EEG segment, we base real-time change detection on a flexible time window containing the last j segments, by testing the hypothesis

$$\begin{cases} H_0 : c_i = C_0 & l-j < i \le l \quad \text{(no change)} \\ H_1 : c_i = C_1 & l-j < i \le l \quad \text{(change)} \end{cases}, \tag{27}$$

where $j \in [J_{\min}\, J_{\max}]$. The optimal solution to the hypotheses testing problem, according to the Neyman–Pearson Criterion (Lehmann 1991), is the likelihood-ratio test. However, for the case at hand, it cannot be implemented due to ignorance of the time of change, the value of C_1 and the noise covariance matrices, $\mathbf{\Sigma}_i$. Instead, we use a two-step GLRT-based detection scheme (Robey et al. 1992). First, we assume that $\mathbf{\Sigma}_i$ is known, and derive the GLRT, in which the unknown parameters are replaced by their ML estimates (Lorden 1971). Then, the sample covariance matrices, $\hat{\mathbf{\Sigma}}_i$, are inserted in place of the true covariance matrices into the test.

Premising that the noise covariance matrices are known, it can be shown by Neyman–Fisher factorization criterion (Fisher 1925) that the ML estimators $(\hat{c}_{l-j+1}, \ldots, \hat{c}_l)$ are sufficient statistics with respect to the parameter C and the raw data segments $(\mathbf{y}_{l-j+1}, \ldots, \mathbf{y}_l)$. Hence, we define the Generalized Likelihood Ratio as a function of j

$$\hat{\Lambda}_l(j) = \frac{\sup_{C_1} p(\hat{c}_{l-j+1}, \ldots, \hat{c}_l | C_1)}{p(\hat{c}_{l-j+1}, \ldots, \hat{c}_l | C_0)}. \tag{28}$$

Assuming that the EEG segments are statistically independent (an assumption which is not entirely valid, but is a good approximation), the Generalized Log Likelihood Ratio is

$$r_j^l = \sup_{C_1} \sum_{i=l-j+1}^{l} \ln \frac{p(\hat{c}_i | C_1)}{p(\hat{c}_i | C_0)}. \tag{29}$$

As the time of change is unknown, we base detection on $G[l]$, an optimization of r_j^l over all the possible values of j

$$\begin{aligned} G[l] &= \max_j r_j^l \\ \text{s.t.} \quad & J_{\max} < j \le J_{\min}. \end{aligned} \tag{30}$$

According to (25), (26) and (29), we get

$$G[l] = \max_j \sup_{C_1} \sum_{i=l-j+1}^{l} \frac{-\left|\hat{c}_i - C_1\right|^2 + \left|\hat{c}_i - C_0\right|^2}{\sigma_i^2}. \tag{31}$$

Finding $\tilde{C}_1(j)$, the supremum of C_1 for each possible value of j, is a convex optimization problem that can be solved by simple derivation. The solution is

$$\tilde{C}_1(j) = \frac{\sum_{i=l-j+1}^{l} \frac{\hat{c}_i}{\sigma_i^2}}{\sum_{i=l-j+1}^{l} \frac{1}{\sigma_i^2}}. \tag{32}$$

After calculating $\tilde{C}_1(j)$, the unknown variance values ${\sigma_i}^2$ are replaced by their estimators, $\hat{\sigma}_i^2$, based on (26).

$G[l]$ is calculated as the solution of the optimization problem:

$$\begin{aligned} G[l] &= \max_j \sum_{i=l-j+1}^{l} \frac{-\left|\hat{c}_i - \tilde{C}_1(j)\right|^2 + \left|\hat{c}_i - C_0\right|^2}{\hat{\sigma}_i^2} \\ \text{s.t.} \quad & J_{\max} < j \le J_{\min}. \end{aligned} \tag{33}$$

As j is a discrete parameter with finite number of possible values, the latter maximization is calculated by comparison of all possible values. The system decides that a change has been detected when $G[l]$ is greater than a pre-defined threshold, λ

$$d[l] = \begin{cases} 0 \text{ if } & G[l] < \lambda \ (H_0 \text{ is chosen}) \\ 1 \text{ if } & G[l] \ge \lambda \ (H_1 \text{ is chosen}) \end{cases}, \tag{34}$$

where λ is chosen to satisfy a robustness criteria, based on our system's performance analysis, which is discussed in the next section (e.g. reducing the probability of false alarms to <0.1 per minute).

4 Simulations and performance analysis

4.1 Simulation details

We analyzed the algorithm's performance using Monte Carlo simulations in which the SSEP were generated as cosine functions. Background EEG activity was simulated as a realization of an AR random process of the form

$$w[n] = \sum_{j=1}^{p} \alpha_j w[n-j] + u[n], \tag{35}$$

where $u[n]$ is white Gaussian noise (Zetterberg 1969, Gersch 1970). The values of the parameters $[\alpha_0, \alpha_1, \ldots, \alpha_p]$ were extracted from real EEG data recorded during anesthesia by Burg method (Kay 1988) for AR model order (P) of 12 (Bender et al. 1992). Samples of our computer-generated EEG and real EEG recorded during steady-state stimulation are plotted in Fig. 4.

Five thousand simulations of 400 s were conducted for each scenario, at a sampling rate of 300 Hz and SSEP frequency of 15 Hz, a typical visual SSEP frequency (Zaaroor et al. 1993). The value before surgery, C_0, was set to 0.15 (SSEP is a cosine function with zero phase and amplitude

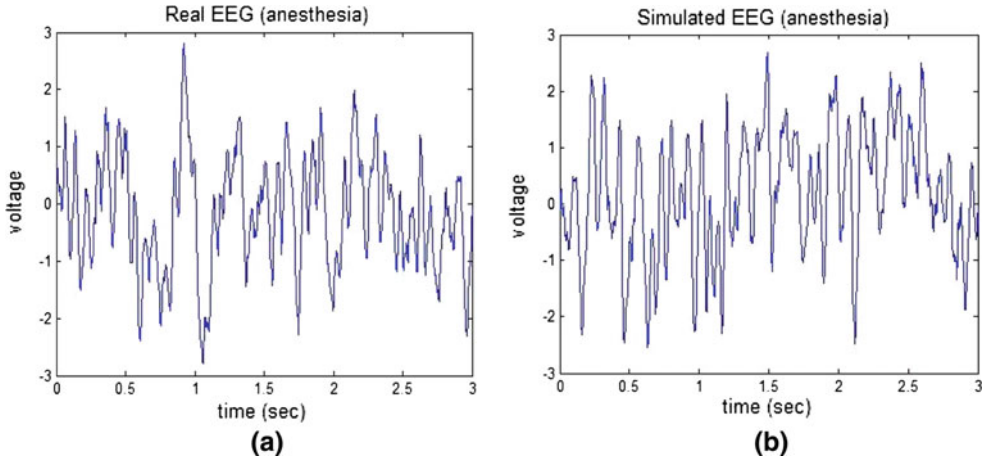

Fig. 4 **a** Real EEG recorded during steady-state stimulation of a comatose patient. **b** Computer-generated EEG (using harmonic signal model and additive autoregressive process of order 12). Sampling rate is 300 Hz, segments duration is 3 s. Signal energy is normalized to 1, SNR is −23 dB

of 0.3). Phase jumps of $\frac{\pi}{4}$ and $\frac{\pi}{2}$ radians, corresponding to changes of $\frac{1}{8}$ and $\frac{1}{4}$ inter-stimulus intervals in the SSEP latency, as well as amplitude changes of −0.1 and +0.2 were simulated after 100 s. The background EEG variance was normalized to 1, producing an SNR of −13 dB, segmentation step was set to a second ($kN_T = 300$) and $J_{\max}$ was set to 90 s. After consulting neuro-physiologists experienced in intra-operative monitoring, the parameter $J_{\min}$ (the minimal number of observations required for detection) was set to 30. This configuration increases the system's robustness and prevents alarms that are based on <30 s of EEG, even when it seems likely that a change has occurred, due to the high cost of distracting the attention of the doctor during brain surgery. A second set of runs was simulated with $C_0 = 0.05$, leading to an SNR of −23 dB. Exemplary simulation outputs are plotted in Fig. 5.

4.2 Performance evaluation

A change detector is a device delivering an alarm signal in time t_a about a change that took place at time $\hat{k}$, with t_0 denoting the starting time for the algorithm (Basseville and Nikiforov 1993). Performance measures are Mean Time between False Alarms (MTFA) and Mean Time for Detection (MTD)

$$\text{MTFA} = E(t_a - t_0|\text{no change}), \tag{36}$$

$$\text{MTD} = E(t_a - \hat{k}|\text{change}). \tag{37}$$

For each threshold, MTFA, MTD and the probability of getting a false alarm in a 60 s simulation (PFA) for all simulated cases are recapitulated in Table 1. Note that some of the values were not calculated due to the rare occurrences of the events. The configuration $\lambda = 13$ was chosen for the purpose of performance analysis, as the lowest threshold for which PFA was below 0.1. Setting the threshold to $\lambda = 13$ provides delay for detection of <21 s for a phase jump as low as $\frac{\pi}{4}$ degrees in −13 dB SNR. For −23 dB SNR, the magnitude of change $|C_1 - C_0|$ is significantly lower due to the smaller SSEP amplitude. In this case, all changes are detectable as well. In the amplitude jump scenario, in which the change magnitude is the same for both SNR cases, MTD reduces with the relative magnitude of change. As a result, MTD values are lower for SNR of −23 dB.

4.3 Comparison with previous methods

All methods discussed in Sect. 2 were simulated, where the manual neuro-physiological change detection was imitated by a post-processing step, of comparing the difference between the estimated signal and the baseline before surgery to a threshold

$$d[l] = \begin{cases} 0 \; if \quad |\hat{C}[l] - C_0| < \Delta \text{ (no change)} \\ 1 \; if \quad |\hat{C}[l] - C_0| \geq \Delta \text{ (change)} \end{cases}, \tag{38}$$

where $\hat{C}[l]$ is the estimated parameter value in the lth time instance. As our algorithm is capable of detecting phase changes of $\frac{\pi}{4}$ in the low SNR scenario without generating false alarms, we chose the threshold as

$$\Delta = |0.05e^{\frac{\pi}{4}i} - 0.05| \approx 0.04, \tag{39}$$

and calculated MTFA for the −23 dB scenario, based on 5,000 simulations for each of four optional estimation time windows (T). The results are summarized in Table 2.

Using the lowest possible values of T in which false alarms are rare (<0.1 in 60 s) in each method, we conducted 5,000 simulations of a $\frac{\pi}{2}$ phase change, for both SNR cases. The threshold was set to

$$\Delta = |C_0 e^{\frac{\pi}{4}i} - C_0|, \tag{40}$$

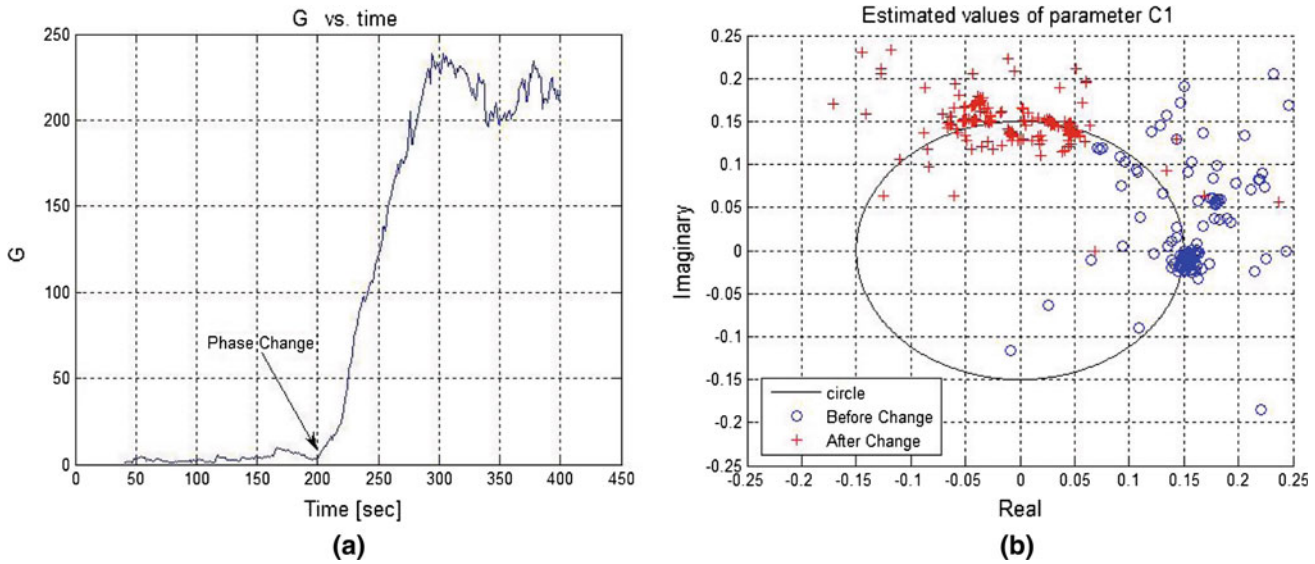

Fig. 5 Computer simulation of SSEP change detection, SNR is −13 dB. **a** A $\frac{\pi}{2}$ radians phase change from the baseline occurs after 200 s, leading to a dramatic increase in the value of the decision parameter $G[l]$ within seconds. **b** Plotted values of parameter C_1, 200 s before (*blue*) and after (*red*) the change. The *black circle* is centered at the origin with a radius of 0.15. It is evident from the estimated values that a phase jump of approximately $\frac{\pi}{2}$ radians have occurred. (Color figure online)

Table 1 PFA (in 60 s), MTFA and MTD of $\frac{\pi}{4}/\frac{\pi}{2}$ radians phase jumps and −0.1/+0.2 amplitude changes for threshold, achieved using our GLRT solution (in seconds)

	−13 dB						−23 dB					
λ	PFA	MTFA	$\pi/4$	$\pi/2$	−0.1	+0.2	PFA	MTFA	$\pi/4$	$\pi/2$	−0.1	+0.2
5	0.62	56.7	8.4	4.8	15.4	11.8	0.43	42.8	36.5	15.6	9.5	18.2
10	0.23	254.6	17.1	9.4	39.1	37.9	0.16	218.7	52.3	23.6	39	18.2
13	0.1	–	20.7	11.3	55.7	52.0	0.07	–	82.9	29.9	33.4	23.8
20	0.02	–	29.3	15.8	106.6	–	0.03	–	187.1	49.5	49.5	32.3
50	0.01	–	69.0	24.6	–	–	0.01	–	–	243.5	93.3	97.9
100	0	–	–	40.6	–	–	0	–	–	–	–	–

Table 2 MTFA (in seconds) for estimation time window in all SSEP estimation methods

T (s)	45	60	90	180
Empirical	8.5	17.7	53.4	266.7
Subspace	250.6	–	–	–
Fourier	150.0	244.7	–	–
Lock-in	284.2	–	–	–

Table 3 MTD for a $\frac{\pi}{2}$ phase change in all SSEP estimation methods

	T (s)	−13 dB	−23 dB
Empirical	180	90.8	72.3
Subspace	60	31.4	32.6
Fourier	90	63.6	63.7
Lock-in	60	42.1	40.6
GLRT	30–90	11.3	29.9

a magnitude of a $\frac{\pi}{4}$ phase change. MTD values for each method are recapitulated in Table 3, where MTD for the GLRT method uses $\lambda = 13$.

The low SNR simulations demonstrate that all methods are superior to the empirical averaging currently used in routine practice. While our algorithm outperforms all other methods, the subspace averaging method is marginally inferior to the GLRT when the estimation time window is well chosen, and the difference may be referred to the fact that our algorithm utilizes prior knowledge about the background EEG statistics. The high SNR simulations, in which our algorithm significantly outperforms all other methods, demonstrates the role of our post-processing step, which bases detection on a flexible time window whose size is not predetermined. This approach maintains the system's reliability in terms of false alarms while reducing delays for detection when possible.

5 Real steady-state evoked potential experiments

Real SSEP data were recorded at the Neurosurgery department in Rambam hospital, Haifa, Israel, using Axon Systems Inc. Epoch XP 2000/Lite Eclipse Neurological Workstation. Procedures were approved by the Human Subjects Institutional Review board according to the Helsinki convention. EEG was recorded during visual steady-state stimulation at a frequency of 14.925 Hz and band pass filtered at 1–80 Hz using a digital Butterworth, LFF 6 dB/octave, HFF 24 dB/octave with a notch at 50 Hz. The raw data were scaled to have a variance of 1, and re-sampled to 597 Hz, to allow segments with an integer number of inter-stimulus periods.

5.1 Normal awake patients

Apart from testing the algorithm, the purpose of the first experiment was verifying that our system records physiological SSEP rather than an artifact generated by the stimulus. Nine minutes (540 s) of potential difference between electrodes Cz-O1 were recorded from normal awake patient (eyes closed). The first 300 s contained visual steady-state stimulus, followed by 2-min break and 3 min in which the stimulating goggles were flipped over, such that the LEDS were facing outside, rather than the eyes. The SSEP baseline before the flip was estimated using subspace averaging, producing SNR of −26 dB, which is lower than the low SNR scenario in our simulations. The values of the change detector $G[l]$ are plotted in Fig. 6a. The value was kept below 15 until the break after 300 s, that resulted an increase of the parameter up to 30. It is evident that the high value was kept during the flipped-goggle simulation, verifying that our recorded signal is not an artifact. Setting an optimal threshold would detect the change within approximately 80 s, without generating false alarm. The experiment was repeated successfully with a different subject in a 360 s SSEP recording, in which the stimulus was turned off after 180 s and was renewed with a flipped goggle after 300 s. The SSEP baseline produced SNR of −10 dB, and optimal threshold would allow detection within 15 s as evident in Fig. 6b. Note that the change detector's value is significantly greater in the second experiment, due to the increased SNR.

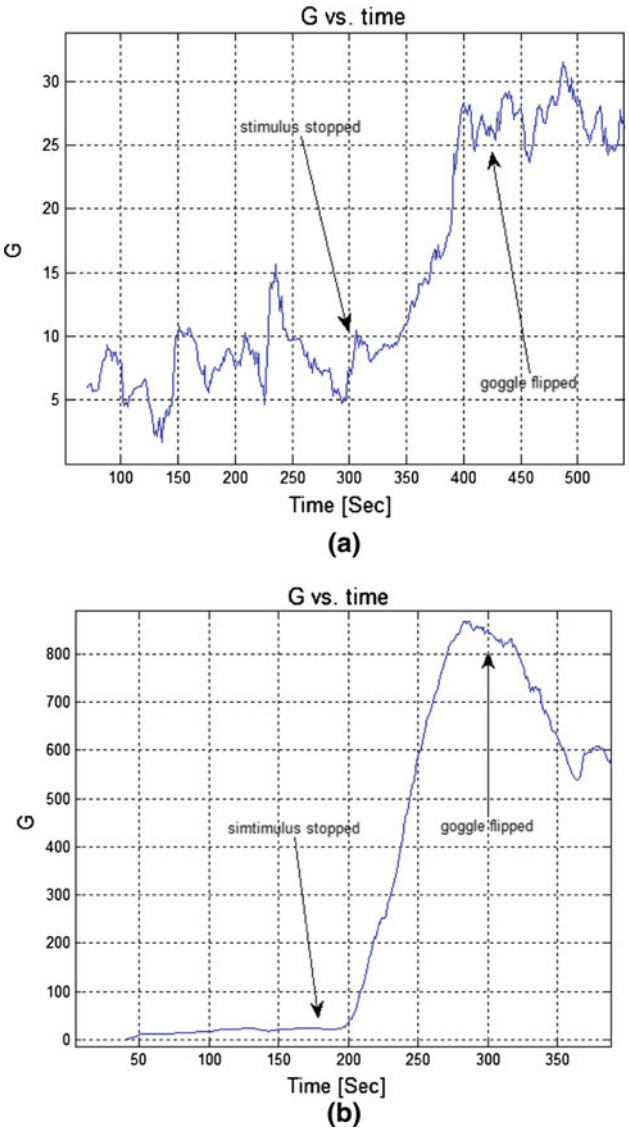

Fig. 6 Change detection of SSEP recorded from awake patients. **a** SNR is −26 dB. After 300 s, the stimulus is turned off and the value of $G[l]$ is increasing due to vanishing of the SSEP. After 420 s the stimulus is turned on with a flipped goggle, with no response. **b** SNR is −10 dB. After 180 s, the stimulus is turned off, followed by an increase of $G[l]$. After 300 s, it is turned on with a flipped goggle, with no response. Note that detection is faster and the parameter $G[l]$'s value is higher in the second experiment due to increased SNR

5.2 Recording during coma

Two hundred seconds of EEG were recorded during steady-state stimulation from a 30 y/o male subject in coma suffering from diffuse axonal injury. Potential difference was recorded between electrodes A1-Oz. The SSEP baseline was estimated using subspace averaging waveforms, in which the presence of harmonic signal with a stable phase was evident. A relative instability of the SSEP amplitude, that varied between 0.25 and 0.3 was observed, in accordance with previous clinical studies (Zaaroor et al. 1993). The amplitude baseline was set to 0.28, producing SNR of −11 dB. Baseline latency was 18 samples, which are approximately 0.03 s corresponding to a phase leg of 162°.

5.2.1 Phase changes

We initially ran the algorithm on the raw EEG data as is. Phase jitters were created by removing 20, 10 and 5 EEG samples after 100 s, corresponding to jumps of π, $\frac{\pi}{2}$ and $\frac{\pi}{4}$ in

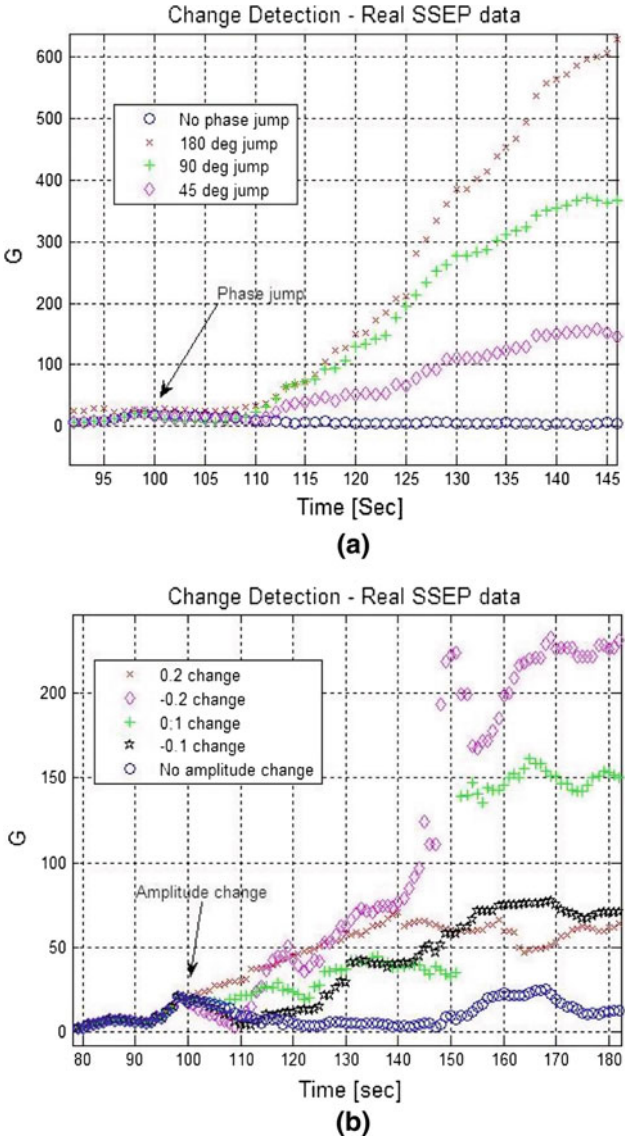

Fig. 7 Change detection of SSEP recorded under coma. **a** Phase jump detection of different values. The maximum value of $G[l]$ observed when no change has occurred is 25. When a phase jump occurs after 100 s, the value of $G[l]$ increases accordingly. It is evident that even a change as low as 45o is detectable. **b** Detection of amplitude changes of different magnitudes. It is evident that for all magnitudes of change, setting a threshold in which no false alarms occur and change is detected within 10–30 s is possible. Note that the amplitude baseline was relatively unstable during the recording, and as a result detection is less reliable

the SSEP phase. The values of $G[l]$ in all cases are plotted in Fig. 7a. The value was kept below 25 when no samples were removed. A phase jump of π resulted in a dramatic increment of up to a hundred within 17 s that kept increasing for 90 s, exceeding 1,200. A $\frac{\pi}{4}$ jump has lead to a more moderate, yet clearly observable increment of $G[l]$ up to a hundred after 30 s, stopping at nearly 200. It is evident that a threshold in which all experimented phase jumps are clearly detected within 10–20 s (depending on the magnitude of change) can be set without generating any false alarms. The maximum value when no change occurs is not as low as expected in our computer simulations, due to the amplitude instability of the real SSEP.

5.2.2 Amplitude changes

Computer-generated cosine functions with the same phase as the SSEP were added to or subtracted from the EEG recording after 100 s, resulting in a change of the SSEP amplitude baseline. The magnitudes of change were ± 0.1 and ± 0.2, which are approximately 35 and 70 % of the original baseline amplitude. $G[l]$'s values are plotted in Fig. 7b. All changes were detected by the algorithm, when the larger change of 0.2 (in both directions) resulted a larger increase of $G[l]$. $G[l]$'s behavior was less predictable in relation to phase changes, due to the instability of the SSEP amplitude of the real data. Yet, setting a threshold that does not generate false alarms and detects all changes within 10–30 s is feasible.

5.2.3 Comparison with previous methods

We tested the performance of the empirical and sub-space averaging methods on the data recorded under coma, using the detector from Eq. (38) and the thresholds from Eqs. (39) and (40). When trying the empirical average on the raw data as is, we could not attain satisfactory PFA for any of the T values we had tried; as our recording lasted 200 s, the maximum averaging window that we tested was 120 s, for which PFA was 0.4. For the sub-space method, setting T to 45 s was enough to prevent false alarms. Using the aforementioned values of T, we tested both methods in the $\frac{\pi}{2}$ and $\frac{\pi}{4}$ phase change scenarios, the results are summarized in Table 4. For comparison, we used the performance of the GLRT with a threshold of $\lambda = 50$, twice the maximal value of the detector in the "no change" scenario. Arguably, the empirical average is not sufficiently sensitive for automated detection due to its high PFA for the case at hand. The sub-space method is adequate for reliable monitoring, although the GLRT performs faster as far as time for detection is concerned.

Table 4 Real data performance: PFA and time for detection (TD, in seconds) for a $\frac{\pi}{2}$ and $\frac{\pi}{4}$ phase change, using different SSEP estimation methods

	T (s)	PFA	TD $\frac{\pi}{2}$	TD $\frac{\pi}{4}$
Empirical	120	0.4	81	95
Subspace	45	0	26	76
GLRT	30–90	0	14	19

Table 5 Computational complexity of the change detection algorithm's different stages

Covariance matrix estimation	$O(kN_t{}^2)$
ML Estimation	$O(kN_t{}^3)$
Calculating $G[l]$	$O(j_{\max}{}^3)$

6 Real-time performance and computational complexity

For a real-time algorithm, computational complexity is an issue. The complexities of each of the algorithm's stages are recapitulated in Table 5. For each segment of kN_t samples (which correspond to 1 s EEG data in our case), we estimate the covariance matrix, a Topeliz matrix with $2p$ different values. The calculation can be performed with complexity of $O(kN_t{}^2)$ by recursively updating the covariance matrix of the previous segment. In addition, we calculate the SSEP ML estimator using matrix inversion and multiplication, with complexity $O(kN_t{}^3)$. The data volume is significantly reduced after the ML estimator is computed, as we use its statistical sufficiency to base detection on the ML estimators, instead of the EEG raw data. Finally, the double optimization over parameter C_1 and the time of change is computed with complexity $O(j_{\max}{}^3)$, and its efficiency may be enhanced using iterative updating methods. Overall, the computational complexity of the GLRT is polynomially dependent on the segmentation size and the time of change optimization length; both are bounded values ($kN_t = 300$ and $j_{\max} = 90$) in our Monte Carlo simulations. A 5-min EEG simulation requires <20 s on a personal computer with a 2-GHz CPU. Performance can be accelerated even further using a real-time digital signal processor (DSP).

7 Conclusion and discussion

We presented a novel algorithm for monitoring the real-time variations of SSEP during neurosurgical procedures. Our approach is based on detecting changes in the SSEP from its baseline before surgery, using a two-step GLRT. The algorithm exploits the harmonic signal model and prior statistical knowledge about spontaneous EEG activity during anesthesia, for conducting an hypothesis test that base detection on a flexible time window. The algorithm is capable of detecting changes in the SSEP within seconds in low SNR conditions, outperforming conventional neurosurgical monitoring methods. In contrast to signal estimation approaches, the algorithm makes decisions based on statistical analysis of the likelihood that a change has occurred rather than manual interpretation, thus enhancing the system's sensitivity and reliability.

The computational complexity of the GLRT is polynomial, making it applicable for real-time implementation. Furthermore, the algorithm was applied successfully to a single EEG channel recording, making it appealing for neurosurgical operations in which placing electrodes on the scalp might be inconvenient or impracticable. As our algorithm is based on a statistical test, expanding the solution to multichannel EEG recordings can be applied by treating each channel as an independent information source, and making a decision based on a majority rule.

Our ability to test the algorithm in real scenarios was limited by ethical considerations, as it requires anesthetized subjects as well as initiating functional changes in the subject's brain. Testing the algorithm on EEG recorded during neuro-surgical procedures in which the times of neurological changes are documented shall be the next step of our clinical trials. Other issues that still require further clinical investigation are the effects of differences in depth of anaesthesia on the SSEP, and the reliability of the signal's amplitude measurements. The amplitude's instability has been documented in previous clinical studies, and yielded performance differences between our real data experiments and the idealized Monte Carlo simulations of our algorithm.

References

Bach MMT, Meigen T (1999) Do's and don'ts in fourier analysis of steady-state potentials. Doc Ophthalmol 99:69–82

Basseville M, Nikiforov IV (1993) Detection of abrupt changes: theory and applications. Prentice-Hall, Englewood Cliffs

Bender R, Schultz B, Schultz A, Pichlmayr I (1992) Testing the gaussianity of the human eeg during anasthesia. Methods Inf Med 31(1):56–59

Bergholz R, Lehmann TN, Fritz G, Ruther K (2008) Fourier transformed steady-state flash evoked potentials for continuous monitoring of visual pathway function. Doc Ophthalmol 116:217–229

Burke D, Nuwer M, Daube J, Fischer C, Schramm J, Yingling CD, Jones S (1999) Intraoperative monitoring. Electroencephalogr Clin Neurophysiol 52:133–148

Chiappa K (1997) Evoked potentials in clinical medicine. Lippincott-Raven, Philadelphia

Davila C, Srebro R (2000) Subspace averaging of steady-state visual evoked potentials. IEEE Trans Bio-Med Eng 47:720–728

Davilla C, Ghaleb I, Serebro R (1997) Prewhitening of background brain activity via autoregressive modeling. Biomedical engineering conference, 1997, Proceedings of the 1997 sixteenth southern pp 242–245

Fisher RA (1925) Theory of statistical estimation. Proc Camb Philos Soc 22:700–725

Friman O, Luth T, Volosyak I, Graser A (2007) Spelling with steady-state visual evoked potentials. 3rd International IEEE/EMBS conference on neural engineering, pp 354–357

Gersch W (1970) Spectral analysis of EEGs by autoregressive decomposition of time series. Math Biosci 7:205–222

Gevins AS (1984) Analysis of electromagnetic signals of the human brain: Milestones, obstacles, and goals. IEEE Trans Biomed Eng 31:833–850

Heckenlively JR, Arden GB (1991) Principles and practice of clinical electrophysiology of vision. Mosby, St Louis

Kay SM (1988) Modern spectral estimation. Prentice-Hall, Englewood Cliffs

Lehmann EL (1991) Testing statistical hypothesis. Statistical/probability series. Wadsworth and Brooks/Cole, Pacific Grove

Lorden G (1971) Procedures for reacting to a change in distribution. Ann Math Stat 42:1897–1908

McGillem CD, Aunon JI, Yu KB (1985) Signal and noise in evoked potentials. IEEE Trans Biomed Eng 32:1012–1016

Middendorf M, McMillan G, Calhoun G, Jones KS (2000) Brain–computer interfaces based on the steady-state visual-evoked response. IEEE Trans Neural Syst Rehabil Eng 8:217–229

Nuwer M, Daube J, Fischer C, Schramm J, Yingling C (1993) Neuromonitoring during Surgery, Report of an IFCN Committee. Electroencephalogr Clin Neurophysiol 87(5):273–276

Nuwer MR, Dawson EG, Carlson LG, Kanim L, Sherman JE (1995) Somatosensory evoked potential monitoring reduces neurologic deficits after scoliosis surgery: Results of a large multicenter survey. Electroencephalogr Clin Neurophysiol 96:6–11

Orfanidis SJ (1996) Optimum signal processing. An introduction. 2. Prentice-Hall, Englewood Cliffs

Pratt H, Matrin WH, Bleich N, Zaaroor M, Shacham SE (1994) High intensity, goggle-mounted flash stimulator for short-latency visual evoked potentials. Electroencephalogr Clin Neurophysiol 92: 469–472

Robey FC, Fuhrmann DR, Nitzberg R, Kelly EJ (1992) A CFAR adaptive matched filter detector. IEEE Trans Aerosp Electron Syst 28:208–216

Schacham SE, Pratt H (1985) Detection and measurement of steady-state evoked potentials using a lock-in amplifier. J Neuroserg 62:935–938

Scofield JH (1994) Frequency-domain description of a lock-in amplifier. Am J Phys 62((2):129–133

Wiedemayer H, Fauser B, Sandalcioglu IE, Armbruster W, Stolke D (2004) Observations on intraoperative monitoring of visual pathways using steady-state visual evoked potentials. Eur J Anaesthesiol 21:429–433

Zaaroor M, Pratt H, Feinsod M, Shacham SE (1993) Real time monitoring of steady-state visual evoked potentials. Isr J Med Sci 29(1):17–22

Zetterberg LH (1969) Estimation of parameters for a linear difference equation wih applications to EEG analysis. Math Biosci 5:227–275